

Article

A New High-Efficiency Double-Stator Split-Pole Permanent-Magnet Vernier Machine with Flux-Focusing Topology

Zhengwen Dai ¹, Jianguo Li ^{1,*}, Lin Zou ¹, Junhua Wang ^{2,*} and Ruiren Luo ¹

¹ School of Mechanical and Electronic Engineering, Wuhan University of Technology, Wuhan 430070, China; dzw2015@whut.edu.cn (Z.D.); l.zou@163.com (L.Z.); ruiren123@whut.edu.cn (R.L.)

² School of Electrical Engineering, Wuhan University, Wuhan 430070, China

* Correspondence: jianguoli@whut.edu.cn (J.L.); junhuawang@whu.edu.cn (J.W.); Tel.: +86-138-7151-2670 (J.L.); +86-27-68776608 (J.W.)

Academic Editor: Eric Ka-wai Cheng

Received: 23 December 2016; Accepted: 29 March 2017; Published: 4 April 2017

Abstract: Permanent-magnet vernier machines (PMVMs) have attracted much attention for their high efficiency and output torque in low-speed application. However, the conventional PMVM suffers from the problems of low power factor and high cogging torque. In this paper, a double-stator flux-focusing split-pole permanent-magnet vernier machine (SP-PMVM) with low cogging torque and high power factor has been proposed. The split-pole topology in the vernier motor has been used mainly to modulate the magnetic flux in this paper, although the stator teeth are used for this purpose in some cases. The newly-proposed SP-PMVM topology is characterized by reduced flux leakage through using a flux-focusing topology and staggering approximately half of the pitch angularly between the inner stator and outer stator. Firstly, the vernier principle of the proposed SP-PMVM has been investigated by analytical methods. Secondly, a 12-slot-stator and 22-pole-pair-rotor SP-PMVM has been optimized with the goal of maximum average steady-state torque and the minimum cogging torque and ripple. Thirdly, the overall performance of the newly-proposed SP-PMVM has been analyzed as compared with the conventional PMVM. The results verify that the SP-PMVM can provide higher power factor, higher output torque and lower cogging torque than that of the conventional PMVM in low-speed application.

Keywords: split-pole; cogging torque; flux-focusing; high-efficiency; permanent-magnet vernier machine; power factor

1. Introduction

In recent years, permanent-magnet vernier machines (PMVMs) have attracted considerable attention because of their favorable characteristics in direct-drive system, such as high torque, high robustness, and simplicity. Many kinds of PMVMs have been proposed by researchers [1,2]. An outer-rotor PMVM, which has low power factor and high cogging torque has been proposed by Li et al. for direct drive [3]. Zhao et al. have proposed a double-stator axial-flux spoke-type PMVM and found that the power factor can be improved by using the spoke PMs [4]. Kim et al. have analyzed the performances of PMVM by analytical method and proposed that larger power factor than that of conventional PMVM can be obtained by selecting slot and pole combinations properly [5]. Nevertheless, the low power factor, which is one of the most significant problems, has not been fully investigated and validated.

The non-negligible cogging torque of PMVM is another problem to be solved. As we know, the cogging torque, which is generated by the interaction between the rotor magnet and the stator teeth in

PMVMs, can cause vibration and noise [6]. Therefore, when the torque variation frequency is the same as the inherent mechanical frequency of the stator or rotor, it will cause a resonance in the machine, which will further increase the vibration and noise. The influence of cogging torque is more obvious especially for the single-air-gap spoke type of conventional PMVMs [7].

In this paper, a double-stator split-pole permanent-magnet vernier machine (SP-PMVM) with a flux-focusing topology, as show in Figure 1, has been proposed to improve the abovementioned problems, namely, low power factor and high cogging torque. Firstly, the vernier principle of the proposed SP-PMVM has been investigated by analytical methods. Secondly, a 12-slot-stator and 44-pole-rotor SP-PMVM has been proposed and optimized based on the maximum average steady-state torque and the minimum cogging torque and ripple. Thirdly, the overall performance of the newly-proposed SP-PMVM has been compared with the conventional PMVM.

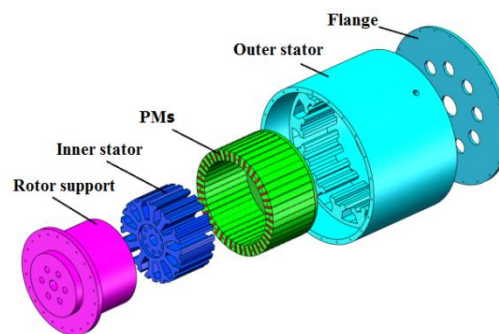


Figure 1. 3D view of the SP-PMVM.

2. Machine Design

2.1. Mechanical Design

The mechanical design of the SP-PMVM is shown in Figure 2. It can be seen that the rotor is sandwiched between the inner stator and outer stator through a rotor bracket and the rotor bracket is combined directly with the output shaft. The inner stator is mounted on a supporter which is bolted to the outer frame. To reduce the deformation of the inner stator supporter shaft, a reinforcing ring is used in this paper. Since the rotor bracket is a torque-transferring part from the rotor to the output shaft, it should have enough mechanical strength.

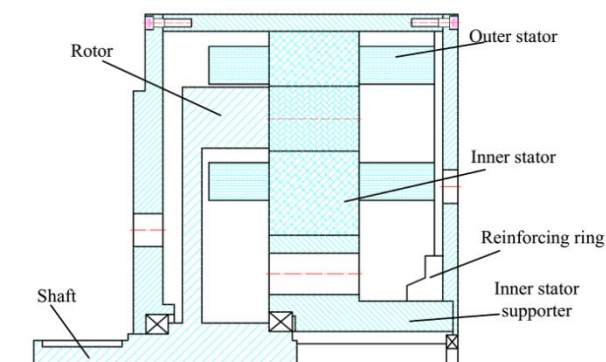


Figure 2. Front view of the SP-PMVM.

2.2. Machine Topology

The cross-sections of conventional PMVM and the newly-proposed SP-PMVM are shown in Figure 3a,b, respectively. The newly-proposed SP-PMVM consists of an inner stator, an outer-stator,

and a cup-rotor. The inner stator has 12 slots, which are imbedded with a three-phase four-pole winding. Each stator tooth is punched into two flux-modulating poles. The outer stator has the same number of slots, winding pole-pairs, and flux-modulating poles as with the inner stator. To minimize the flux leakage, the inner stator and outer stator are staggered by about half of the pitch, angularly. The cup rotor is composed of 44-pole permanent-magnet bulks which are fixed on a cup-shaped bracket. The cup-rotor is sandwiched between the inner-stator and outer-stator.

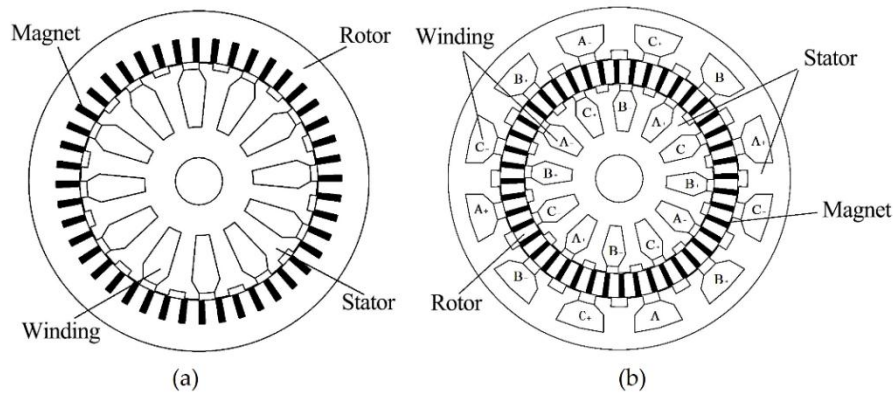


Figure 3. Comparison of the two machines: (a) conventional PMVM; and (b) SP-PMVM.

For a PMVM with full pitch windings, the stator slot N_S can be represented by $6pq$, where q is the number of slots per pole per phase. If the relationship of Equation (1) is satisfied, the vernier effect is built up [8]:

$$N_R = N_S \pm P \tag{1}$$

where N_R , N_S , and P are the number of rotor magnet pole-pair number, flux-modulating pole number, and winding pole-pair number, respectively. The relationship of Equation (1) is the key to obtaining the vernier effect and high-torque low-speed characteristic.

3. Theoretical Analysis

Before the analysis, the definition of the key parameters of SP-PMVM should be given, which are shown in Figure 4. It should be noted that the predefined positive rotating direction of stator is counter-clockwise.

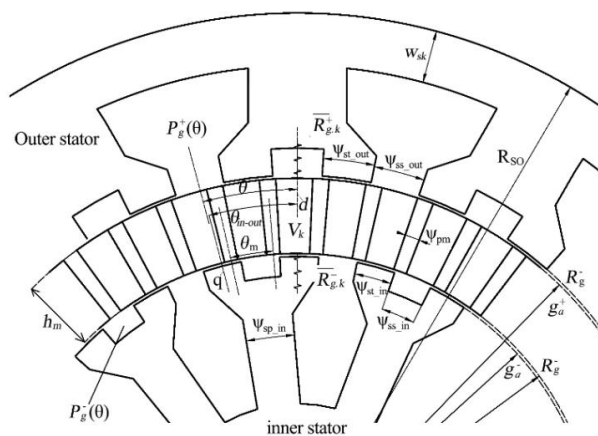


Figure 4. Definition of parameters of SP-PMVM.

To calculate the flux density and the permeance, the rotor can be divided into 44 pieces, angularly, and the magnetic circuit of each piece is shown in Figure 5. The potential along the edge facing the

outer air gap is magnetically floating and the magnetic potential of each piece could be calculated. In the figure, V_k is the potential of k^{th} rotor piece, F_{mag} is the MMF of permanent magnet, R_m is the lump reluctance of a permanent magnet and $\overline{P}_{g,k}$ is the lumped air gap permeance facing the k^{th} rotor piece.

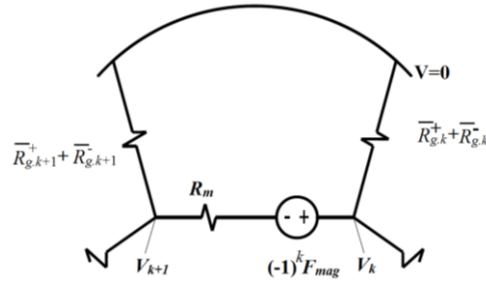


Figure 5. Magnetic circuit of one section in the rotor of SP-PMVM.

Since the inner stator is shifted by half of the pitch relative to the outer stator, the outer air gap and inner air gap specific permeance [9,10], $P_g^\pm(\theta)$ is given in Equation (2):

$$P_g^\pm(\theta) = P_0^\pm \mp P_1^\pm \cos(N_S\theta) \tag{2}$$

where the quantities P_0^\pm is the average permeance, P_1^\pm is the fundamental permeance, and θ is the angle of air gap of angular position.

In order to utilize the vernier effect and to avoid MMF oscillation and loss of permeability [11], the rotating MMF and the air-gap flux density are given by Equations (3) and (4):

$$F_{g.PM}^\pm(\theta) = \frac{4}{\pi} \frac{F_{mag}}{2 + R_m \overline{P}_0} \cos(N_R(\theta - \theta_m)) \tag{3}$$

where $F_{g.PM}^\pm$ is the MMF developed by PM, \overline{P}_0 is the permeance of a core piece, θ is the angle of air gap of angular position, and θ_m is the angle between the rotor permanent magnet. The air-gap flux density are given by Equation (4):

$$B^\pm(\theta) = \frac{4B_r h_m}{\pi \mu_m (2 + R_m \overline{P}_0)} \cos(N_R(\theta - \theta_m) (P_0^\pm \mp P_1^\pm \cos(N_S\theta)) \tag{4}$$

where B_r is the residual flux density of PM, h_m is the rotor permanent magnet thickness, and μ_m is the permeability of permanent magnet.

By using Equation (4), the back-EMF (rms) of a phase winding induced in outer stator with q slots per pole per phase and N_{ph} turns can be simplified, as in Equation (5):

$$E_{cp-pmvm} = \frac{4l_{sk}\omega_m}{\sqrt{2}\pi} B_r D_g^+ (k_w N_{ph}) \varepsilon_{E.cp-pmvm} \tag{5}$$

where l_{sk} is the stack length of core, ω_m is a mechanical rotor speed, D_g^+ is the air gap diameter, k_w is a slot space factor, N_{ph} is a slot space factor, and $\varepsilon_{E.cp-pmvm}$ is the back EMF coefficient of the SP-PMVM motor.

4. Premise for Fair Comparison

To investigate the validity of the newly proposed SP-PMVM, it is optimized and compared with the conventional PMVM machine proposed in [3], as shown in Figure 3a.

It is necessary to explain some key design data and coefficients in the following optimization and comparison:

1. The original parameters of both machines are defined as shown in Figure 4. Other main parameters are listed in Table 1.
2. Some original dimensions and parameters should be defined and explained. ψ_{ss_in} and ψ_{ss_out} are the pole-arc to pole-pitch ratios of the inner and outer stators, respectively; ψ_{st_in} and ψ_{st_out} are the stator tooth width of the inner and outer stators, respectively. The ψ_{pm} is the rotor PM width in degrees, and these parameters are used to define the coefficients:

$$k_{st} = \varphi_{st_in} / \varphi_{s_np} = \varphi_{st_out} / \varphi_{s_np} \tag{6}$$

$$k_{rt} = \varphi_{pm} / (\varphi_{pm} + \theta_m) \tag{7}$$

where $\varphi_{s_np} = \varphi_{st_in} + \varphi_{ss_in} = \varphi_{st_out} + \varphi_{ss_out}$.

3. The β_s is the original rotor module tooth width, which satisfies:

$$\beta_s = 360^\circ / P / N_s = 360^\circ / 2 / 24 = 7.5^\circ \tag{8}$$

Here, θ is twice of the β_s , so $\theta = 2 \times \beta_s = 15^\circ$, and β_{mec} is defined as the mechanical angle between the outer stator teeth and the inner stator teeth [12], which can be described as:

$$\beta_{mec} = \theta - \theta_{in-out} \tag{9}$$

where θ_{in-out} is the angle between d -axis and q -axis (in Figure 4).

4. In addition, to analysis the cogging torque, the rotor speed is set as 1 rpm and all armature winding current are set as zero [13].

Table 1. Design data comparison of PMVM and SP-PMVM.

Items	PMVM	SP-PMVM
Number of rotor pole pairs N_R	22	22
Number of stator slots N_S	24	24
Winding pole-pairs P	2	2
Based speed n_b (rpm)	150	150
Stack length, l_a (mm)	84	84
Outer radius of outer rotor (stator), R_{so} (mm)	144	144
Inner radius of outer rotor (stator), R_{sin} (mm)	100.8	100.8
Stator yoke length, w_{sk} (mm)	2.6	2.6
Yoke angle, ψ_{st_in} (deg)	8	8
Shaft radius, R_{shaft} (mm)	10	10
PM thickness, h_m (mm)	10	10
PM width, g_m (mm)	2.5	2.5
Air gap length, g (mm)	0.4	0.4
Maximum current, I_{max} (A)	24.4	24.4
Motor power, χ (kW)	5.88	14
Stator turns per coil, N_{tpc}	15	25
Number of slots per pole per phase, N_p	1	1
Wire per conductor, N_w	1	1
Slot space factor β	0.65	0.65
Wires size (AWG)	19	19
Iron type	DW310_35	the same
PM type	NdFe30	the same
Shaft material	45Cr	the same
Motor weight (kg)	38.45	34.93

For fair comparison, the following assumption is made. Namely, the two machines are designed with the same: (a) overall dimensions, such as the stator outer diameter and stack length; (b) base speed, and load ratings; (c) phase current and current density [14,15]; and (d) number of PMs.

5. Optimization of SP-PMVM

The T_{avg} capability, the cogging torque T_{cog} , and the torque ripple T_{ripple} are the most important performances to be considered in the following optimization of the SP-PMVM. From the analysis above, the key parameters, such as k_{st} , β_{mec} , h_m , and k_{rt} , are optimized finite element method (FEM) software, while other parameters of the SP-PMVM are kept constant, as listed in Table 1.

5.1. Optimize k_{st}

It should be noted that the inner stator and outer stator have consistent coefficients, namely, $\psi_{st_in} = \psi_{st_out}$, while optimizing k_{st} . In addition, the split ratio can be defined as:

$$k_o = R_{shaft} / R_{so} \tag{10}$$

The value k_o of SP-PMVM is -0.15 . The coefficient k_{st} is optimized in the FEM software at $I_{max} = 24.4$ A, and ψ_{st_in} and $\psi_{st_out} = 1^\circ - 7^\circ$. The k_{st} is changed from 0.2–0.55 while keeping other parameters constant, as listed in Table 1.

The results of average torque, cogging torque, and torque ripple at different k_{st} are shown in Figure 6. It can be seen that when the coefficient k_{st} is about 0.4, the T_{avg} is at the maximum value. However, the tendencies of T_{cog} and T_{ripple} curves are not quite similar with T_{avg} . When k_{st} is about 0.47, T_{ripple} reaches the minimum value. At this point, the T_{avg} decreases by 25% from the peak point and the T_{cog} is decreased by 30%.

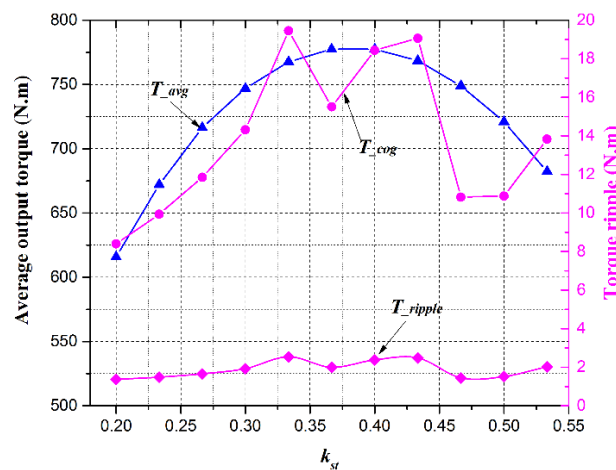


Figure 6. Average torque, cogging torque, and torque ripple of SP-PMVM at different k_{st} .

From the above discussion, the optimization is a compromise between average output torque and torque ripple. When the coefficients of $k_{st} = 0.46$, a large torque can be obtained and the torque ripple is acceptable. Consequently, $k_{st} = 0.46$ is adopted in this stage and used for the next step.

5.2. Optimize β_{mec}

Since the angle β_{mec} has a great influence on T_{avg} , the power factor and the T_{ripple} of the SP-PMVM, the mechanical angle β_{mec} is optimized in the range of $-2.5^\circ - 5^\circ$ in the FEM software, while other parameters are kept constant, as listed in Table 1.

Figure 7 shows the results of the average torque, cogging torque and torque ripple at different β_{mec} . It can be found that the maximum torque is obtained at 0° . The T_{cog} and T_{ripple} almost reach the minimum values at this point as well. Hence, this point, namely $\beta_{mec} = 0$, $k_{st} = 0.46$, and $k_{rt} = 0.3$, is better than initial values which are given in Table 2. Additionally, this set of parameters will be used for the following analysis and optimization.

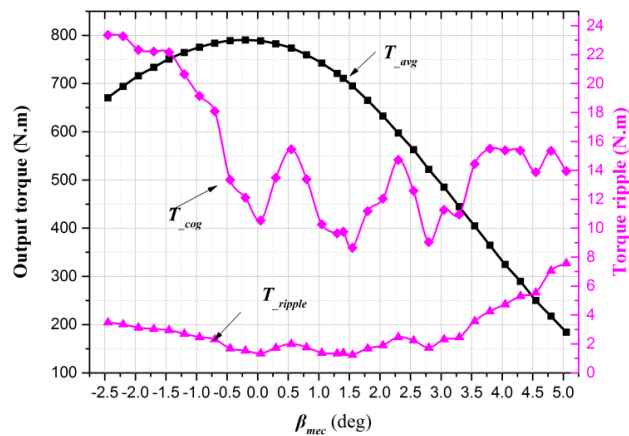


Figure 7. Average torque, cogging torque, and torque ripple at different β_{mec} .

Table 2. Optimized Dimension of SP-PMVM.

Items	Initial Value	Optimized Value
k_{st}	0.46	0.46
k_{rt}	0.3	0.3
β_{mec} (deg)	1	0
T_{avg} (N.m)	750	800
T_{cog} (N.m)	10	10.5
T_{ripple} (%)	1.33	1.31
h_m (mm)	10	10

5.3. Optimize k_{rt} and h_m

To obtain the region of maximum average torque with a variety of optimal PM size, the parameters k_{rt} and h_m are investigated by the FEM calculation. Based on optimized dimension of the SP-PMVM in the last two steps, its average torque, cogging torque, and torque ripple are investigated when k_{rt} and h_m are in the range of 0.1–0.5 and 3–15 mm, respectively. Other parameters are kept the same as the original ones which are given in Table 1.

The average torque at different k_{rt} and h_m is shown in Figure 8. It demonstrates that the area of maximum T_{avg} can be obtained is in the region γ , which is defined between the contour Line a and b. Line a corresponds to the parameters of k_{rt} and h_m in the range of 0.2–0.4 and from 10–15 mm, respectively.

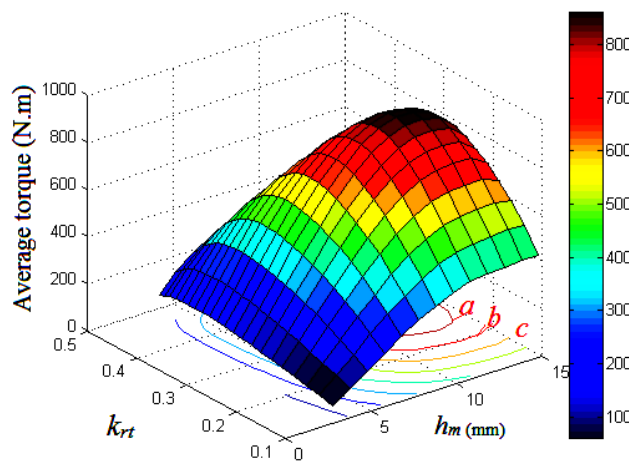


Figure 8. Average torque at different k_{rt} and h_m .

Figure 9 shows the cogging torque at different k_{rt} and h_m . It can be seen that the influence of the coefficient k_{rt} on T_{cog} is irregular, but the T_{cog} is sensitive to the h_m . Moreover, it also can be found that the peak T_{cog} falls in the γ area.

Furthermore, the torque ripple at different k_{rt} and h_m is investigated, as shown in Figure 10. It shows that, as compared with the influence of h_m , the T_{ripple} is more sensitive to the k_{rt} . As long as it remains in the γ region, the T_{ripple} is not very large. This indicates that although the T_{cog} reaches the highest value in the γ area, the T_{avg} and T_{ripple} reach in the maximum value and minimum value, respectively. Therefore, we will adopt the design in the γ region because the SP-PMVM has good torque performance and the torque ripple is quite acceptable in this area.

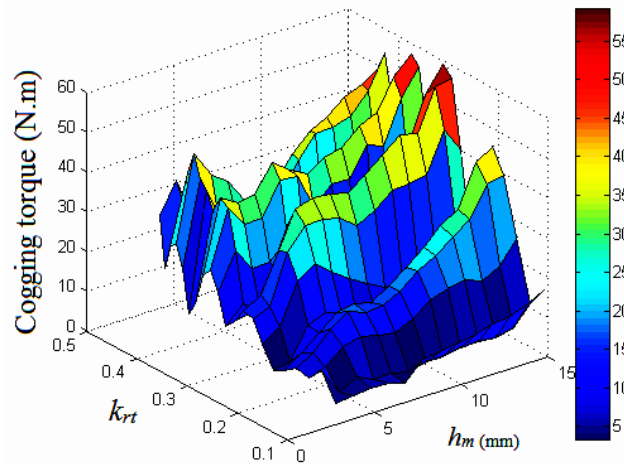


Figure 9. Cogging torque at different k_{rt} and h_m .

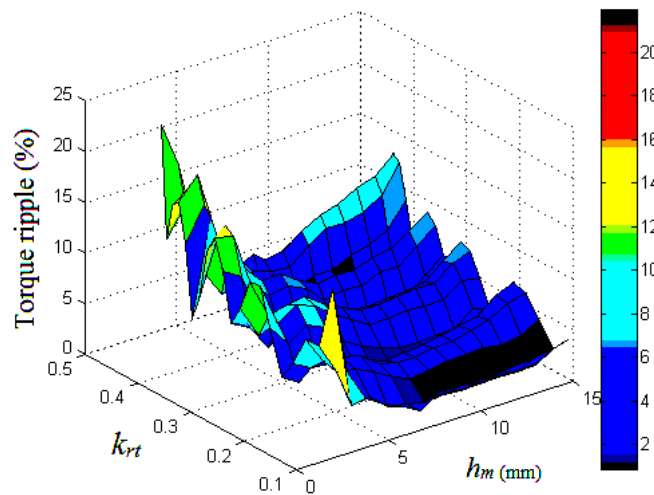


Figure 10. Torque ripple at different k_{rt} and h_m .

6. Performance Comparison

Some parameters may affect the electromagnetic performance to a large extent, such as k_{st} , β_{mec} , h_m , and k_{rt} . With the assumptions that the steel saturation is ignored and the permeability of permanent magnet is the same as the air, the magnetic field distribution of the conventional PMVM and the SP-PMVM are given in Figure 11a,b, respectively. This shows that more flux links between the rotor and stator of the newly-proposed SP-PMVM form than that of the conventional PMVM under the same condition. This is mainly owing to the improved magnetic path of the SP-PMVM by shifting the relative position of the inner stator and outer stator and the adopting of a flux-focusing topology.

The outer air-gap flux density of the conventional PMVM and the SP-PMVM are calculated by a time-stepping finite-element method (TS-FEM) at no-load, as shown in Figure 12. It can be noted that the flux density of the conventional PMVM is much smaller than that of the SP-PMVM with the same number of PMs. Quantitatively, the maximum outer air-gap flux density of the conventional PMVM and SP-PMVM are 0.944 T and 1.8 T, respectively. The flux linkage of the conventional PMVM at no-load is much smaller than that of the SP-PMVM, as shown in Figure 13. The flux linkage of the SP-PMVM is almost twice that of the conventional PMVM. It should be noted that the power factor of the proposed SP-PMVM is 0.87, as listed in Table 3, which is much larger compared with that of the conventional PMVM (about 0.4). One of the reasons of the improved flux density, the flux linkage and the power factor is that the magnetic flux leakage of the SP-PMVM is much less than the conventional PMVM owing to the shift angle between the inner stator and outer stator of the SP-PMVM. Other reasons may include that the PMVM model based on the original design by other researchers, whereas the SP-PMVM is optimized. It should also be noticed that the data calculated by 2D TS-FEM might be higher than the actual value because the end effect is not considered.

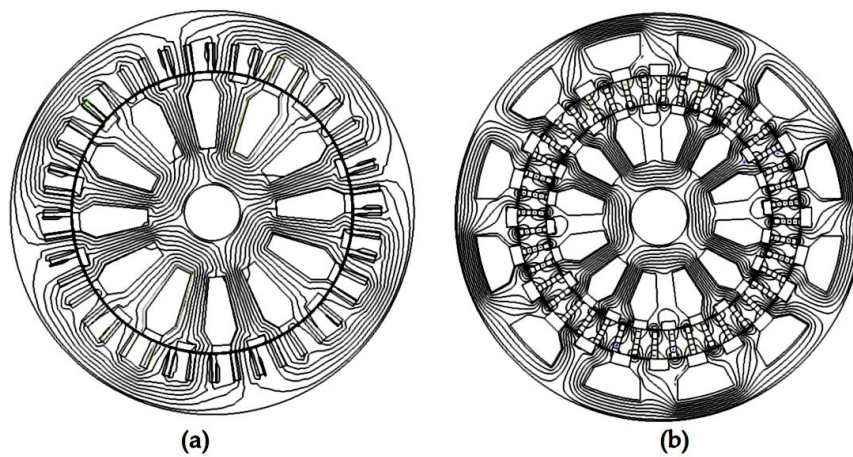


Figure 11. Magnetic field distribution: (a) conventional PMVM; and (b) SP-PMVM.

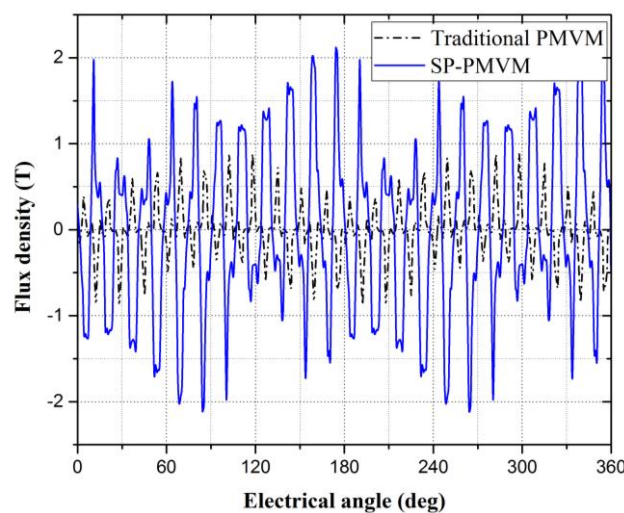


Figure 12. Air gap flux density.

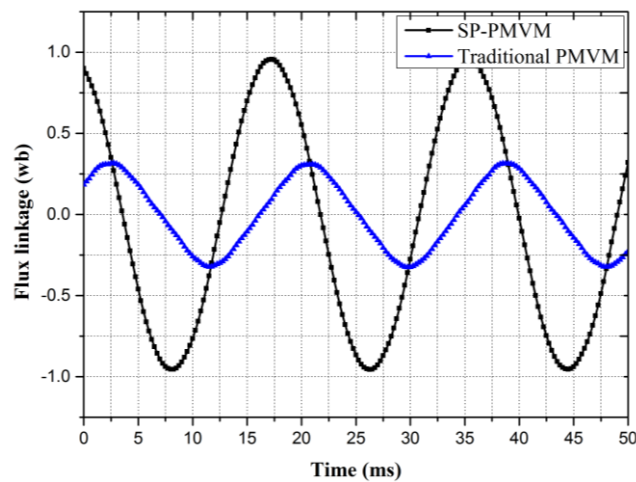


Figure 13. Flux linkage.

Table 3. Optimized Parameters.

Items	Conventional PMVM	Proposed SP-PMVM
k_{st}	0.46	0.46
k_{rt}	0.3	0.3
β_{mec} (deg)	-	0
I_{max}	24.4	24.4
h_m (mm)	12	12
T_{avg} (N.m)	235	800
T_{cog} (N.m)	28	10.5
T_{ripple} (%)	12.7	1.31
Power factor	0.4	0.87
Efficiency	63%	91%
Shear stress (kN/m ²)	40	93
Torque density (N·m/cm ³)	0.14	0.49

Figure 14 shows the no-load cogging torque waveform of the two machines, while the speed of the motor is set as 1 rpm. The peak to peak values of cogging torque T_{cog} and the torque ripple percentage T_{ripple} of both machines are listed in Table 3. It can be seen that the T_{ripple} of the proposed SP-PMVM is 1.31%, which is much lower than that of the conventional PMVM. Therefore, the cogging torque and torque ripple can be reduced by using the proposed design structure.

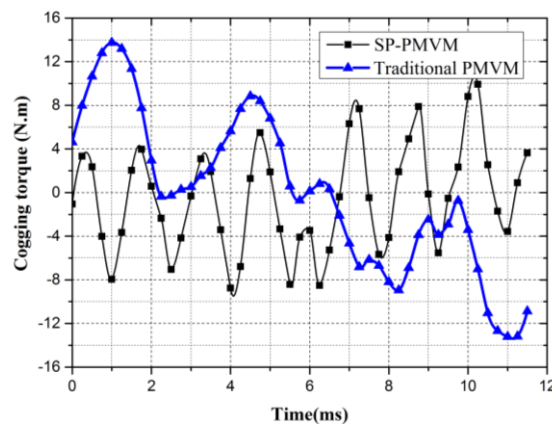


Figure 14. Cogging torque.

Additionally, the steady-state average torque T_{avg} is shown in Figure 15. It can be found that the averaged steady-state torque of proposed SP-PMVM is 800 N·m, while for the conventional PMVM is 235 N·m, namely, the torque-handling ability of the proposed machine is 319% higher than the conventional PMVM.

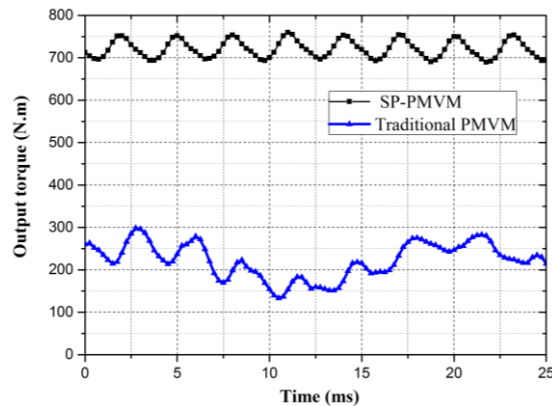


Figure 15. Output torque.

According to above analysis, the power factor, torque, and efficiency are improved to a great extent. The reasons for lower torque ripple, improved output torque, and efficiency may include,

- The SP-PMVM has two air gaps instead of one; therefore, the active area of the machine is almost doubled.
- Comparing with the conventional PMVM with a low power factor (about 0.3–0.6 [8]), the SP-PMVM topology can improve the power factor significantly by staggering about half of the pitch angularly between the inner stator and outer stator.
- Comparing with the conventional PMVM, the magnetic flux leakage of the SP-PMVM has been reduced significantly.

7. Conclusions

In this paper, a new double-stator SP-PMVM with a flux-focusing topology has been proposed. The performances of the SP-PMVM have been optimized and compared with the conventional PMVM. The results show that the SP-PMVM has more favorable characteristics than the previously-designed PMVM. To summarize, the advantages of SP-PMVM are listed as follows:

1. The torque-handling ability is improved by 240%. The output torque per kg PM of the SP-PMVM is about 2.4 times of that of the conventional PMVM.
2. The power factor, which is one of the most significant problems of PMVM, has been improved from about 0.4 to 0.87. For the same current, the SP-PMVM has a lower requirement on the battery for electric drive vehicles (EDVs).
3. The torque ripple is induced from 12.7% to 1.31%. This may broaden the potential application area of the SP-PMVM.

Acknowledgments: This work was supported in part by the Young Scientists Fund of the National Natural Science Foundation of China (project no. 51507122) and the Fundamental Research Funds for the Central Universities (project no. 2017IVA012, 2017zy042).

Author Contributions: Zhengwen Dai mainly conducted the simulation and comparison of the PMVM and SP-PMVM. Jianguo Li conceived and directed the design. Lin Zou and Junhua Wang improved and revised the manuscript. Ruiren Luo analyzed some data. All of the authors contributed to the paper writing.

Conflicts of Interest: The authors declare no conflict of interest.

References

1. Gu, C.Y.; Zhao, W.X.; Zhang, B.F. Simplified minimum copper loss remedial control of a five-phase fault-tolerant permanent-magnet vernier machine under short-circuit fault. *Energies* **2016**, *9*, 860. [[CrossRef](#)]
2. Yang, H.; Lin, H.Y.; Zhu, Z.Q.; Fang, S.H.; Huang, Y.K. A dual-consequent-pole vernier memory machine. *Energies* **2016**, *9*, 134. [[CrossRef](#)]
3. Li, J.G.; Chau, K.T.; Jiang, J.Z.; Liu, C.H.; Li, W.L. A new efficient permanent-magnet vernier machine for wind power generation. *IEEE Trans. Magn.* **2010**, *46*, 1475–1478. [[CrossRef](#)]
4. Zhao, F.; Lipo, T.A.; Kwon, B. A novel dual-stator axial-flux spoke type permanent magnet vernier machine for direct drive applications. *IEEE Trans. Magn.* **2014**, *50*, 1–4. [[CrossRef](#)]
5. Kim, B.; Lipo, T.A. Operation and design principles of a PM vernier motor. *IEEE Trans. Ind. Appl.* **2014**, *50*, 3656–3663. [[CrossRef](#)]
6. Hwang, S.M.; Eom, J.B.; Jung, Y.H.; Lee, D.W. Various design techniques to reduce cogging torque by controlling energy variation in permanent magnet motors. *IEEE Trans. Magn.* **2001**, *37*, 2806–2809. [[CrossRef](#)]
7. Li, D.W.; Qu, R.H.; Thomas, A.L. High-power-factor vernier permanent-magnet machines. *IEEE Trans. Ind. Appl.* **2013**, *50*, 3664–3674. [[CrossRef](#)]
8. Toba, A.; Ohsawa, H.; Suzuki, Y.; Miura, T.; Lipo, T.A. Experimental evaluations of the dual-excitation permanent magnet vernier machine. In Proceedings of the IEEJ 2000 International Analog VLSI Workshop, Stockholm, Sweden, 2–3 June 2000.
9. Kim, B.T.; Lipo, T.A. Analysis of a PM Vernier motor with spoke structure. *IEEE Trans. Ind. Appl.* **2015**, *52*, 217–225. [[CrossRef](#)]
10. Liber, F.; Matt, D. High performance vernier reluctance magnet machine. Application to electric vehicle. In Proceedings of the EPE'95 6th European Conference on Power Electronics and Applications, Sevilla, Spain, 19–21 September 1995; pp. 2889–2894.
11. Toba, A.; Lipo, T.A. Generic torque-maximizing design methodology of surface permanent-magnet vernier machine. *IEEE Trans. Ind. Appl.* **2000**, *36*, 1539–1546.
12. Hua, W.; Cheng, M.; Zhu, Z.Q.; Howe, D. Analysis and optimization of back EMF waveform of a flux-switching permanent magnet motor. *IEEE Trans. Energy Convers.* **2008**, *23*, 727–733. [[CrossRef](#)]
13. Fu, W.N.; Ho, S.L. A quantitative comparative analysis of a novel flux-modulated permanent-magnet motor for low-speed drive. *IEEE Trans. Magn.* **2010**, *46*, 127–134. [[CrossRef](#)]
14. Cao, R.W.; Jin, Y.; Zhang, Y.; Huang, W. A new general design method of segmented-rotor wound field flux-switching motors with complementary magnet circuit. In Proceedings of the 2015 IEEE International Magnetism Conference, Beijing, China, 11–15 May 2015.
15. Bai, J.G.; Zheng, P.; Cheng, L.M.; Zhang, S.K. A new magnetic-field modulated brushless double-rotor machine. *IEEE Trans. Magn.* **2015**, *51*, 1–4.

